Hindawi
Advances in Civil Engineering
Volume 2022, Article ID 3673438, 16 pages
https://doi.org/10.1155/2022/3673438

Research Article

Evaluation of Existing Bond-Slip Relations for CFRP-Steel Joints and New Model for Linear and Nonlinear Adhesives

Mohammed J. Altaee,[1] **Sarmed A. S. Altayee**,[2] **Majid M. A. Kadhim**,[3] **Akram Jawdhari**,[4] **Ali Majdi**,[5] **Ali Chabuk**,[6] **and Nadhir Al-Ansari**[7]

[1]*Environmental Research and Studies Centre, University of Babylon, Hilla, Iraq*
[2]*Department of Chemical Engineering, College of Engineering, University of Babylon, Hilla 51001, Iraq*
[3]*Department of Civil Engineering, College of Engineering, University of Babylon, Hilla 51001, Iraq*
[4]*Department of Civil Engineering, Queen's University, Kingston, Canada*
[5]*Building and Construction Techniques Engineering, Al-Mustaqbal University College, 51001, Babylon, Iraq*
[6]*Department of Environment Engineering, College of Engineering, University of Babylon, Hilla 51001, Iraq*
[7]*Department of Civil Environmental and Natural Resources Engineering, Lulea University of Technology, Lulea 97187, Sweden*

Correspondence should be addressed to Nadhir Al-Ansari; nadhir.alansari@ltu.se

Received 30 March 2022; Accepted 1 July 2022; Published 20 July 2022

Academic Editor: Paolo S. Valvo

Existing bond-slip (τ-s) relations for fibre-reinforced polymer (FRP)-steel joints employ different shapes and mathematical expressions, inferring that their predictions of failure load and mode, and other interface properties, might be inconsistent or inaccurate. In this study, predictions of four widely used τ-s relations are evaluated using a large experimental database of 78 double-lap FRP-steel specimens. To facilitate the evaluation process, a robust finite element (FE) model is developed for each test, implementing data from either of the existing τ-s relations to define the FRP-steel interface. Comparisons between test and FE results indicated that the existing τ-*s* models were unable of predicting the ultimate load (Pu) and effective bond length (L_{eff}) of FRP-steel joints, or the relation between Pu and bond length and that between L_{eff} and FRP modulus (E_f). A new τ-s model is developed based on an inverse FE simulation, comparison with experimental results, and regression analysis. It considers the effects of E_f, the type of FRP reinforcement (sheet or plate), and applies to both linear and nonlinear adhesives. The model predictions were validated by comparing with results from small bond tests and large FRP-strengthened steel beams tested under bending, yielding excellent results for Pu, failure mode, and all other interfacial properties.

1. Introduction

Approximately 9% of the 614,387 bridges in the United States are designated as structurally deficient [1], of which over 52% have steel superstructures [2]. While repair and strengthening of metallic structures have historically been carried out using bolting or welding of steel plates, the use of advanced fibre-reinforced polymer (FRP) composites became a more viable alternative [2–4]. This is because of FRP's desirable properties of high strength-to-weight ratio, corrosion resistance, and ease of transportation, handling, and installation. Of the different available FRP types, carbon-FRP (CFRP) has been heavily used in the retrofit of steel members due to its higher relative stiffness and excellent fatigue performance [2, 3]. CFRP materials are typically classified as standard modulus (SM), high modulus (HM), and ultra-high modulus (UHM) when their modulus of elasticity is less than 200 GPa, 200–400 GPa, or higher than 400 GPa, respectively [3].

Many research studies have explored experimentally the effects of strengthening or repairing steel beams and steel-concrete composite girders [3, 5–7] by adhesively bonding CFRP plates. For example, Fam et al. [3] used CFRP plates with elastic moduli varying from 200 to 400 GPa to strengthen

Table 1: Existing bond-slip models for FRP-steel joints.

Variable	Xia and Teng [11]	Fawzia et al. [16]	Fernando [17]	Wang and Wu [18]
$\tau_{\max}$	$0.8\sigma_{\mathbf{max}}$	$\sigma_{\mathbf{max}}$	$0.9\sigma_{\mathbf{max}}$	$0.9\sigma_{\mathbf{max}}$
s_1	$\tau_{max}t_a/G_a$	$t_a/10$	0.081 mm	$2.6\sigma_{max}/G_a t_a^{0.34}$
s_2	—	—	0.80 mm	$180t_a^{0.4}R^{1.7}/\sigma_{\max} + 0.85t_a^{0.34}\sigma_{\max}/G_a$
sf	$2G_f/\tau_{\max}$	$t_a/4\sigma_{\max}(t_a = 0.1 - 0.5mm)$ $0.125 + t_a - 0.5/10\sigma_{\max}\ t_a = 0.5 - 1.0mm$	$2(G_f - \tau_f(s_2 - \frac{s_1}{2}))/\tau_f + \delta_2$	$360t_a^{0.4}R^{1.7}/\sigma_{\max} + 1.7t_a^{0.34}\sigma_{\max}/G_a$
G_f	$31(\sigma_{\max}/G_a)^{0.56}t_a^{0.27}$	$0.5\,\tau_{\max}\,s_1 + 0.5\,\tau_{\max}\,s_f$ (a)	$628\,t_a^{0.5}R^2$	$243t_a^{0.4}R^{1.7}$

R = tensile strain energy of adhesive, t_a = adhesive thickness, G_a = adhesive shear modulus; $\tau_{\max}$ = maximum interfacial shear stress; s_1 = maximum elastic slip; s_2 = maximum plastic slip; s_f = slip at failure; G_f = interfacial fracture energy. [(a)]Fracture energy represents the area under the bond-slip curve.

three large-scale girders and repair 15 small-scale beams and reported 51 and 19% increase in flexural strength and stiffness, respectively, for the girders. In small beams with completely severed tension flanges, CFRP repair resulted in recovering up to 79% of strength before flange damage. Tavakkolizadeh and Saadatmanesh [5] and Al-Saidy et al. [6] also reported 44 to 76% increase in ultimate strength in composite girders strengthened with SM-CFRP and HM-CFRP plates.

In Peiris [2] and Peiris and Harik [4], UHM-CFRP strip panels were used in strengthening wide flange steel beams and single-span steel-girder bridges. Typical failure modes in SM-CFRP plates include debonding at adhesive-steel or adhesive-CFRP interfaces, cohesive failure within the adhesive layer, and CFRP delamination or rupture [3, 8]. For HM and UHM plates, rupture has been predominately reported, likely because of their lower ultimate strain and thinner section, resulting in smaller normal (peeling) and shear stresses at termination points [9]. While most research on steel strengthening has focused on SM-CFRPs, HM and UHM-CFRPs can provide better utilization of the CFRP material since they allow more load transfer to occur before yielding the steel beam [4, 8–10].

The behaviour of the strengthened member depends greatly on the effectiveness of the bonded joint in transferring loads between the steel member and FRP reinforcement and maintaining composite action, prior to desired failures. Thus, many studies were carried out on the interfacial behaviour of FRP-steel joints, mostly utilizing either single- or double-shear tests [11–15]. From these tests, an interfacial model relating the shear stress (τ) developed in the joint to the slip (s) between the two adherents is developed and presented. The τ–s relation can be used in analytical and numerical studies to evaluate the behaviour of strengthened members and assist in determining several key design results such as ultimate load, bond (development) length, and bond strength.

Several τ-s models have been suggested in previous research studies for the FRP debonding from metallic substrates [11, 16, 17]. Typically, most available models depend on the adhesive's properties such as its tensile strength (σ_max), thickness (t_a), shear modulus (G_a), and fracture energy (G_f), and whether it is brittle (linear) or ductile (nonlinear). Although several shapes were proposed for τ-s relation, exponential and multi-linear, bilinear, and trapezoidal ones constitute the most available and widely used ones. Multiple studies deployed the empirical τ-s models in the analysis and modelling of FRP-bonded steel members.

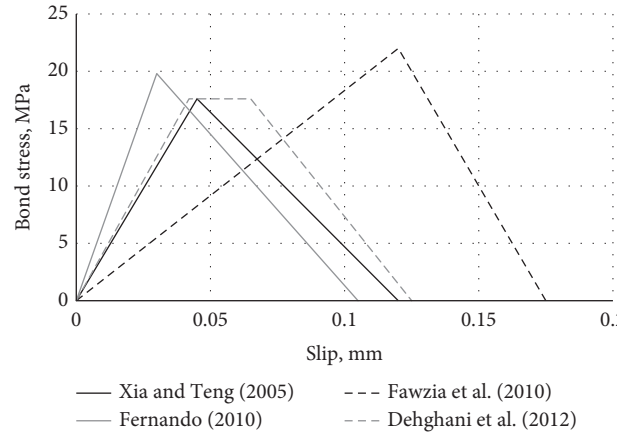

Figure 1: Existing bond-slip models for FRP-steel joints.

2. Existing Bond-Slip Models

Table 1 summarizes the existing bond-slip models for CFRP-steel joints available in the literature. Although other models might also be available, those in Table 1 represent the most widely used and cited ones. These models were developed based on the results of single- or double-lap shear joints containing a steel plate bonded on one or two faces to CFRP sheets or plates. Generally, two types of models can be found in the literature, namely, bilinear models (triangle) and trilinear models (trapezoidal) (Figure 1). The difference between the two shapes is due to using either linear or nonlinear adhesive material, where the former has been reported to result in a bilinear τ–s shape and the latter to give a trilinear bond-slip shape. The following sections discuss the models developed by various researchers, their theoretical composition, strengths, and weaknesses.

While numerous efforts have been put into developing the bond-slip relations for CFRP-steel joints, Table 1 and Figure 1 show that existing models employ different stress-slip relations and mathematical expressions, suggesting that their predictions of failure load, mode, and other interface properties might be inconsistent. This study leverages a nonlinear FE analysis and a large experimental database comprising 78 double-lap joints collected from literature to evaluate predictions of existing τ–s relations for FRP-steel joints and identify the best and worst performing ones.

Based on the numerical results, a parametric study using FE simulations, and regression analysis, a new bond-slip model was developed and presented, providing much better predictions than most existing models. The model considers the effects of different parameters such as FRP modulus and type, adhesive thickness, and fracture energy and applies to both linear and nonlinear adhesives. Predictions of the proposed model have been validated by comparing with experimental results from bond and flexural beam tests.

2.1. Xia and Teng's [11] Model. Xia and Teng [11] carried out a bond study on FRP-steel joints, using the adhesive types (A, B, and C) and four adhesive thicknesses (ta), 1, 2, 4, and 6 mm. The study proposed a bilinear relationship for the bond-slip behaviour for all adhesive types. Table 1 shows the mathematical formulation for Xia and Teng model for the key parameters, τ_max, s_1, s_2, s_f, and G_f, that define the τ–s relation. These parameters are a function of the adhesive thickness, its maximum tensile strength, and shear modulus (Table 1).

2.2. Fawzia et al.'s [16] Model. This study investigated the bond behaviour of CFRP-steel joint, using experimental and finite element results. To achieve a good understanding of the bond performance, several parameters were explored, namely, adhesive type (Sikadur 30, MBrace saturant, and Araldite 420), number of FRP layers (3 and 5), and FRP type (normal modulus and high modulus). Two values for the thickness of steel plates, 6 and 10 mm, were also investigated with a bond length ranging from 80 to 250 mm. Based on their testing and modelling protocol, the study proposed a bilinear bond-slip model, which is shown schematically in Figure 1 and a mathematical representation in Table 1. Like the previous model, the key parameters defining this model are also related to the mechanical properties of adhesive.

2.3. Fernando's [17] Model. Fernando [17] also examined experimentally the bond-slip curve for CFRP-steel joint in terms of the effects of FRP modulus, adhesive type, and adhesive thickness. A single-shear pull-off test method was calibrated and found to be accurate for investigating the pure shear joint behaviour. The results showed that the bond strength depends significantly on the interfacial fracture energy of the adhesive layer. Nonlinear adhesives with lower moduli but larger failure strain are found to result in much higher interfacial fracture energy than linear adhesives. The shape of the τ–*s* model is found to be triangular and trapezoidal for Sikadur (linear) and Araldite (nonlinear) adhesives, respectively. Theoretical expressions were developed for the triangular and trapezoidal τ–s models and were used in an analytical study for predicting the full-range bond behaviour of FRP-steel joints, including estimating the effective bond length. Expressions for the trapezoidal model are shown in Table 1.

2.4. Wang and Wu's [18] Model. Wang and Wu [18] conducted 13 single-shear tests on CFRP-steel joints and evaluated the effects of adhesive properties and thickness. They also reached the same conclusion in Fernando's [17] study regarding the shape of τ–s model concerning adhesive type. Expressions were developed for the bilinear and trapezoidal bond-slip models for Sikadur 30 and Araldite 2015, respectively, based on fitting with the 13 experiments tested by the authors and 37 additional ones collected from the literature. The trapezoidal model by Wang and Wu is shown mathematically in Table 1, and it depends on adhesive properties, namely, σ_{max}, t_a, G_a, and the tensile strain energy of adhesive (R), which relates to the adhesive type (linear vs. nonlinear).

3. Summary of Experimental Studies

A large experimental database comprising 78 specimens was compiled in this study and used to examine the predictive capability of existing bond-slip models. To achieve this goal, a three-dimensional FE model was created for each of the test samples, implementing either of the four of the τ–*s* models discussed above for the steel-FRP interface.

Table 2 lists the collected test specimens, their geometric and material properties, and key experimental results. Al-Mosawe et al. [19] tested 33 double-lap of CFRP-steel specimens and evaluated the effects of FRP modulus (E_f), varying E_f from 159 to 450 GPa corresponding to three moduli (low, normal, and ultra-high), and bond length (L_f), varying L_f from 30 to 130 mm. The specimens comprise a 10 mm thick steel plate bonded to two CFRP laminates that are 1.2–1.4 mm thick (t_f). The adhesive agent bonding the two adherents together was Araldite 420, a 0.5 mm thick nonlinear type. The results showed that debonding of FRP laminate was the dominant failure mode for specimens with low and normal moduli, while for those with ultra-high modulus, FRP rupture governed the behaviour.

Wu et al. [20] also conducted double-lap tests to investigate the behaviour of CFRP-steel bonded joints. UHM-CFRP laminates, with an $E_f = 460$ GPa and $t_f = 1.45$ mm, were used and were bonded to steel using two types of adhesive, Araldite 420 and Sikadur 30. The study evaluated the effects of adhesive properties, bond length, and laminate thickness as listed in Table 2. The study reported that FRP delamination or rupture was the governing failure mode in specimens with Araldite 420 adhesive compared with debonding failure (hereafter debonding failure referring to interface failure) for those with Sikadur adhesive. Also, Araldite 402 helped to achieve higher strength due to its much larger elongation deformation at break compared with Sikadur adhesive. It should be noted that only specimens bonded with Araldite 420 are presented in Table 2.

The third group in Table 2 is the 20 quasi-static double-lap specimens tested by Al-Zubaidy et al. [21]. The primary variables were L_f (bond length), which varied from 10 to 100 mm, and several FRP layers, either one or three. The study revealed that an increasing number of FRP plies contributed to increasing joint strength. Observed failures were FRP debonding for lengths shorter than the effective bond length (L_{eff}) and FRP rupture when L_f was longer. L_{eff} was estimated to be 30 and 50 mm for 1 ply and 3 FRP plies,

Table 2: Geometric and material properties of bond specimens collected from the literature.

Ref.	Specimen ID	CFRP properties			Adhesive properties			Experimental results	
		L_f (mm)	W_f (mm)	E_f (GPa)	T_f (mm)	E_a (GPa)	T_a (mm)	Failure load (kN)	Failure mode
Al-Mosawe et al. [19]	S3-30	30	20	159.4	1.4	1.9	0.5	41	DB*
	S3-40	40						50.7	
	S3-50	50						60	
	S3-60	60						69.1	
	S3-70	70						76.5	
	S3-80	80						86.8	
	S3-90	90						93.6	
	S3-100	100						100.3	
	S3-110	110						108	
	S3-120	120						108.7	
	S3-130	130						109.2	
	NS-30	30						41.9	
	NS-40	40						51.7	
	NS-50	50						60.7	
	NS-60	60						69.8	
	NS-70	70						75	
	NS-80	80						87.4	
	NS-90	90						94.2	
	NS-100	100						101.3	
	NS-110	110						108.3	
	NS-120	120						108.5	
	NS-130	130						109.2	
	UHS-30	30						31.8	
	UHS-40	40						43.3	DL
	UHS-50	50						54.4	
	UHS-60	60						64.1	
	UHS-70	70						73.2	
	UHS-80	80						73.2	
	UHS-90	90						73.2	
	UHS-100	100						73.2	R*
	UHS-110	110						73.2	
	UHS-120	120						73.2	
	UHS-130	130						73.2	
Wu et al. [20]	A30	30	50	478.7	1.45	1.9	0.35	72.8	DL
	A50	50					0.36	137.2	
	A70	70					0.34	178.9	
	A100	100					0.31	250.6	
	A120	120					0.36	271.2	
	A250	250					0.38	267.3	R
	A260	260					0.39	274.9	

Table 2: Continued.

Ref.	Specimen ID	CFRP properties			Adhesive properties			Experimental results	
		L_f (mm)	W_f (mm)	E_f (GPa)	T_f (mm)	E_a (GPa)	T_a (mm)	Failure load (kN)	Failure mode
Al-Zubaidy et al. [21]	CF-1-A-10	10	50	205	0.176	1.45	0.5	19.84	DB
	CF-1-A-20	20						37.87	
	CF-1-A-30	30						45.22	
	CF-1-A-40	40						44.06	
	CF-1-A-50	50						47.44	
	CF-1-A-60	60						46.17	R
	CF-1-A-70	70						46.33	
	CF-1-A-80	80						48.18	
	CF-1-A-90	90						45.82	
	CF-1-A-100	100						46.73	
	CF-3-A-10	10	50	205	3 × 0.176	1.45	0.5	29.6	DB
	CF-3-A-20	20						54.2	
	CF-3-A-30	30						68.88	
	CF-3-A-40	40						82.88	
	CF-3-A-50	50						96.83	
	CF-3-A-60	60						101.35	
	CF-3-A-70	70						103.24	R
	CF-3-A-80	80						97.4	
	CF-3-A-90	90						97.38	
	CF-3-A-100	100						99.22	
Fawzia et al. [16]	NA80	80	50	240	0.57	1.45	0.47	86.1	DB/DL
	NA150	150						77.8	
	NA200	200						92.2	
	NA250	250						93.2	
	HA200	200	50	640	0.95	1.45	0.47	60	R
Nguyen et al. [22]	CF1-20	20	50	240	0.18	1.9	0.5	33.7	DB/DL
	CF1-40	40						46.5	
	CF1-60	60						45.5	
	CF1-80	80						53.1	
	CF3-10	10	50	240	3 × 0.18	1.9	0.5	29.7	
	CF3-20	20						51.5	
	CF3-30	30						66.8	
	CF3-40	40						78.2	
	CF3-50	50						100.9	
	CF3-60	60						96.0	
	CF3-70	70						97.1	
	CF3-90	90						91.2	
	CF3-100	100						98.2	

*DB = FRP debonding; DL = FRP delamination; R = FRP rupture.

respectively. Fawzia et al. [16] also tested several adhesively bonded double-lap joints and studied the effects of L_f for normal ($E_f = 240$ GPa) and high ($E_f = 640$ GPa) modulus CFRP, varying L_f from 80 to 250 mm, and thickness of steel plate. The results showed a mixture of failure modes, with debonding and FRP delamination as the dominant ones. Nguyen et al. [22] also performed experiments on a series of FRP-steel bond specimens using one and three FRP layers and a wide range of bond lengths (Table 2).

4. Finite Element Modelling

The general purpose ABAQUS software V6.16 [34] was used in this study to examine the numerical response of FRP-steel interfaces and bond-slip models presented in Section 2. The explicit solver was selected due to its efficiency and capability of overcoming convergence problems particularly when contact or highly nonlinear behaviour is present. Each model imitated the geometric and material properties of the specimens in Table 2, as they were given in the experimental references.

Due to the symmetry of the double-lap joint in terms of material, loading, and geometry and to reduce computational work, only one-eighth of the full-size specimen was modelled. At the respective planes of symmetry, proper translational and rotational constraints were imposed. The model was fixed by imposing translational longitudinal constraints into the CFRP plate and loaded by applying an incremental longitudinal displacement into the steel plate. A mesh sensitivity study was conducted to choose the optimal mesh size using several sizes including 5, 2, 1, and 0.5 mm. This was conducted for the bond region, while the rest of the specimens had a 5 mm mesh size. A fine mesh, with a maximum element length of 1 mm, was used for all parts (steel, FRP, cohesive elements) inside the bonded region and was gradually increased to 5 mm long elements for other regions (Figure 2). The adhesive layer was modelled by cohesive elements, which were bonded to the steel or FRP parts by master-slave contact, assuming the adhesive layer is the slave entity, and the latter two parts are the master entity.

4.1. Element Selection. The FRP-steel joint consists of three main parts: steel, adhesive, and FRP. Among the different elements that are available in ABAQUS, appropriate ones have been selected for each part depending on the recommendations of previous studies conducted on similar joints [8, 13, 23]. Solid elements C3D8R were employed in the modelling of the steel plate. Linear three-dimensional four-node shell elements S4R with reduced integration were used for modelling FRP, while eight-node three-dimensional cohesive elements, COH3D8, were used in modelling the adhesive layer.

4.2. Material Modelling

4.2.1. Steel. A linear elastic material model was selected for the steel part, using an elastic modulus (Es) of 200 GPa and Poisson's ratio (ν) of 0.3. This model was used because, in all experimental specimens in Table 2, the steel plate was behaving elastically and did not experience yielding or permanent deformations. In addition, the value of elastic modulus was assumed since, in most of the simulated experimental studies, the elastic modulus of steel was not provided.

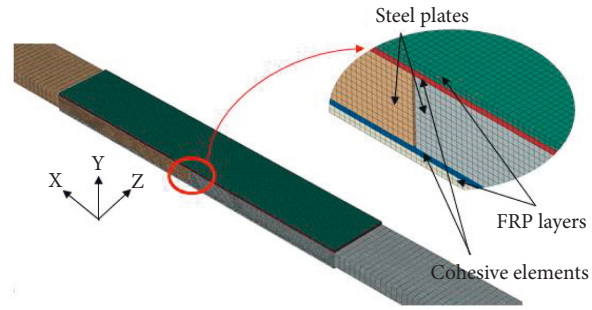

Figure 2: Typical FE mesh for FRP-steel double strap joints (full-size specimen).

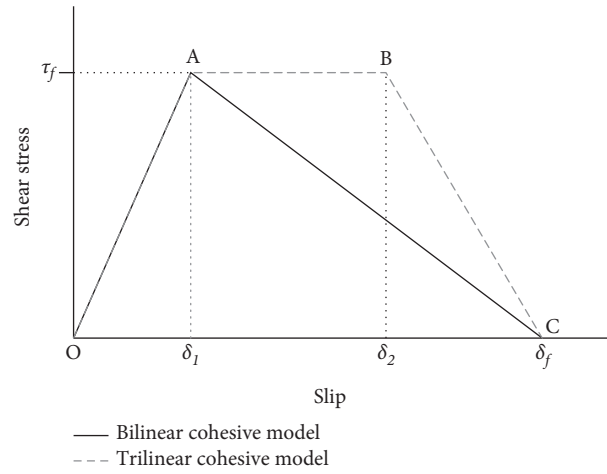

Figure 3: Schematics for bilinear and trapezoidal traction-separation (bond-slip) models implemented in ABAQUS.

4.2.2. CFRP. Like most unidirectional FRP composites simulated in ABAQUS [24], the CFRP plate/sheet was modelled as an orthotropic lamina with linear elastic properties. The FRP rupture failure that occurred in several specimens, particularly those with bond lengths greater than L_{eff}, is explicitly simulated in this study, using Hashin's failure criteria [25].

4.2.3. Cohesive Zone Material. The behaviour of cohesive elements has been captured using the traction-separation law in ABAQUS that is widely used for modelling debonding in FRP-steel or FRP-concrete joints [9, 13, 23]. This model comprises three stages, linear elastic response, damage initiation criterion, and damage evolution law as shown in Figure 3, and discussed in the following sections:

(1) Elastic stage: during the first elastic region (segment O-A in Figure 3), stress increases linearly with

displacement until the damage initiation criterion is activated when the stress reaches the prescribed strength value. The moduli for the elastic portion are defined by three stiffness values, K_{nn}, K_{ss}, and K_{tt}, which can be calculated as follows:

$$\mathbf{K_{nn}} = \frac{\mathbf{E_a}}{\mathbf{t_a}}, \tag{1}$$

$$\mathbf{K_{ss}} = \mathbf{K_{tt}} = \frac{\mathbf{G_a}}{\mathbf{t_a}}, \tag{2}$$

where K_{nn}, K_{ss}, and K_{tt} are the elastic stiffness values for the normal and two shear directions, respectively; E_a and G_a are Young's and shear moduli for the adhesive layer, respectively; and t_a is the thickness of the cohesive element (or adhesive layer). For the specimens in Table 2, E_a, G_a, and t_a were taken from the experimental reference corresponding to each sample.

(2) Damage initiation criteria: the damage criterion is a quadratic stress failure expression (QUADSCRT), which considers the mixed mode, normal (mode I) and shear (mode II) of failure. It is assumed that the damage is initiated when the following equation is satisfied:

$$\left\{\frac{\mathbf{t_n}}{\mathbf{t_n^o}}\right\}^2 + \left\{\frac{\mathbf{t_s}}{\mathbf{t_s^o}}\right\}^2 + \left\{\frac{\mathbf{t_t}}{\mathbf{t_t^o}}\right\}^2 = 1, \tag{3}$$

where $\mathbf{t_n}$, $\mathbf{t_s}$, and $\mathbf{t_t}$ are the stresses in three orthotropic directions in the adhesive layer, and $\mathbf{t_n^o}$, $\mathbf{t_s^o}$, and $\mathbf{t_t^o}$ are the adhesive strengths in the same respective axes.

(3) Damage evolution law: once the damage initiation occurs, the last stage (damage evolution) begins signalling cumulative degradation in the stiffnesses of the cohesive elements and progression of debonding. This stage is represented by line AC for the bilinear model or by the two lines AB and BC for the trilinear model (Figure 3).

The damage variable (D) is implemented in ABAQUS to define the damage evolution and is calculated in two different ways depending on the shape of the bond-slip model (bilinear or trilinear). For bilinear bond-slip models such as Xia and Teng [11] and Fawzia et al. [16], D can be evaluated as follows:

$$\mathbf{D} = \frac{\mathbf{s_m^f}\left(\mathbf{s_m^{max}} - \mathbf{s_m^1}\right)}{\mathbf{s_m^{max}}\left(\mathbf{s_m^f} - \mathbf{s_m^1}\right)} \mathbf{for} \mathbf{s_m^1} < \mathbf{s_m^{max}} < \mathbf{s_m^f}. \tag{4}$$

Since there are only three traction-separation laws available in ABAQUS, which are the bilinear, exponential, and tabular traction-separation laws, therefore the trilinear (trapezoidal) bond-slip models, such as Fernando [17] and Wang and Wu [18], cannot be implemented directly into ABAQUS. However, the tabular cohesive model functionality can be used to implement the damage variable (D) for the trilinear law.

The damage variable of the trapezoidal law was derived by the authors using the values calculated from (5). This equation is derived based on a careful technical review of ABAQUS's theory manual [24]. ABAQUS evaluates the stress in the cohesive element through the equation $t_x = (1 - D)\bar{t}_x$, where x represents the mode (n for mode I; s for mode II; and t for mode III) and t_x represents the stress in the cohesive element, while $\bar{t}_x$ is stress predicted by the elastic behaviour for the current strains without damage. Since the elastic behaviour stress is evaluated as $\bar{t}_x = K_x s_m^{\max}$, Eq (5) is derived to retain a damage variable (when $s_m^{\max}$ is greater than s_m^1 and less than s_m^2) that results in constant stress evaluated by ABAQUS, which is equal to τ_f, and a material softening when $s_m^{\max}$ is greater than s_m^2 and less than s_m^f.

$$\mathbf{D} = \begin{cases} 1 - \dfrac{\mathbf{s_m^1}}{\mathbf{s_m^{max}}} \text{ if } \mathbf{s_m^1} < \mathbf{s_m^{max}} < \mathbf{s_m^2} \\ 1 - \left(\left(\dfrac{\mathbf{s_m^1}}{\mathbf{s_m^{max}}}\right)\left(\dfrac{\left(\mathbf{s_m^f} - \mathbf{s_m^{max}}\right)}{\left(\mathbf{s_m^f} - \mathbf{s_m^2}\right)}\right)\right) \text{ if } \mathbf{s_m^2} < \mathbf{s_m^{max}} < \mathbf{s_m^f} \end{cases}, \tag{5}$$

where s_m^{max} is the maximum value of the effective displacement at any point in the traction-separation response; s_m^1 is the effective displacement at the point of damage initiation (when (3) is satisfied), and s_m^2 is the displacement at which the material deterioration starts. The effective displacement, s_m, is a function of separation in the normal direction and slipping in both shear directions and can be determined from the following equation:

$$\mathbf{s_m} = \sqrt{\mathbf{s_n^2} + \mathbf{s_s^2} + \mathbf{s_t^2}}, \tag{6}$$

where s_n, s_s, and s_t are separation in the normal and both shear directions, respectively, at any point in the traction-separation response.

The evolution law is defined by specifying the difference between s_m at failure completion (s_m^f) and s_m at initiation stage (s_m^1) damage, $[s_m^f - s_m^1]$, for the bilinear bond-slip model, or $[s_m^f - s_m^2]$, for the trapezoidal bond-slip model. Values of $s_m^f - s_m^1$ or $s_m^f - s_m^2$ have been divided into 200 points to create an accurate tabular cohesive zone model. The model is introduced into ABAQUS through a table containing three variables: D, s_m, and mode mix ratio, which is calculated as follows [24]:

$$\begin{aligned} &\mathbf{ModeMixratio\,(bilinearmodel)} \\ &= \frac{\mathbf{GS}}{\mathbf{GT}}, \mathbf{ModeMixratiofor\,(trilinear\,model)} = \frac{\mathbf{G_t}}{\mathbf{GS}}, \end{aligned} \tag{7}$$

where GS and GT can be calculated as follows:

$$\mathbf{GS} = \mathbf{G_s} + \mathbf{G_t}, \tag{8}$$

$$\mathbf{GT} = \mathbf{G_n} + \mathbf{G_s} + \mathbf{G_t}, \tag{9}$$

where G_n is fracture energy in the normal direction (mode I); G_s is fracture energy in the first shear direction (mode II);

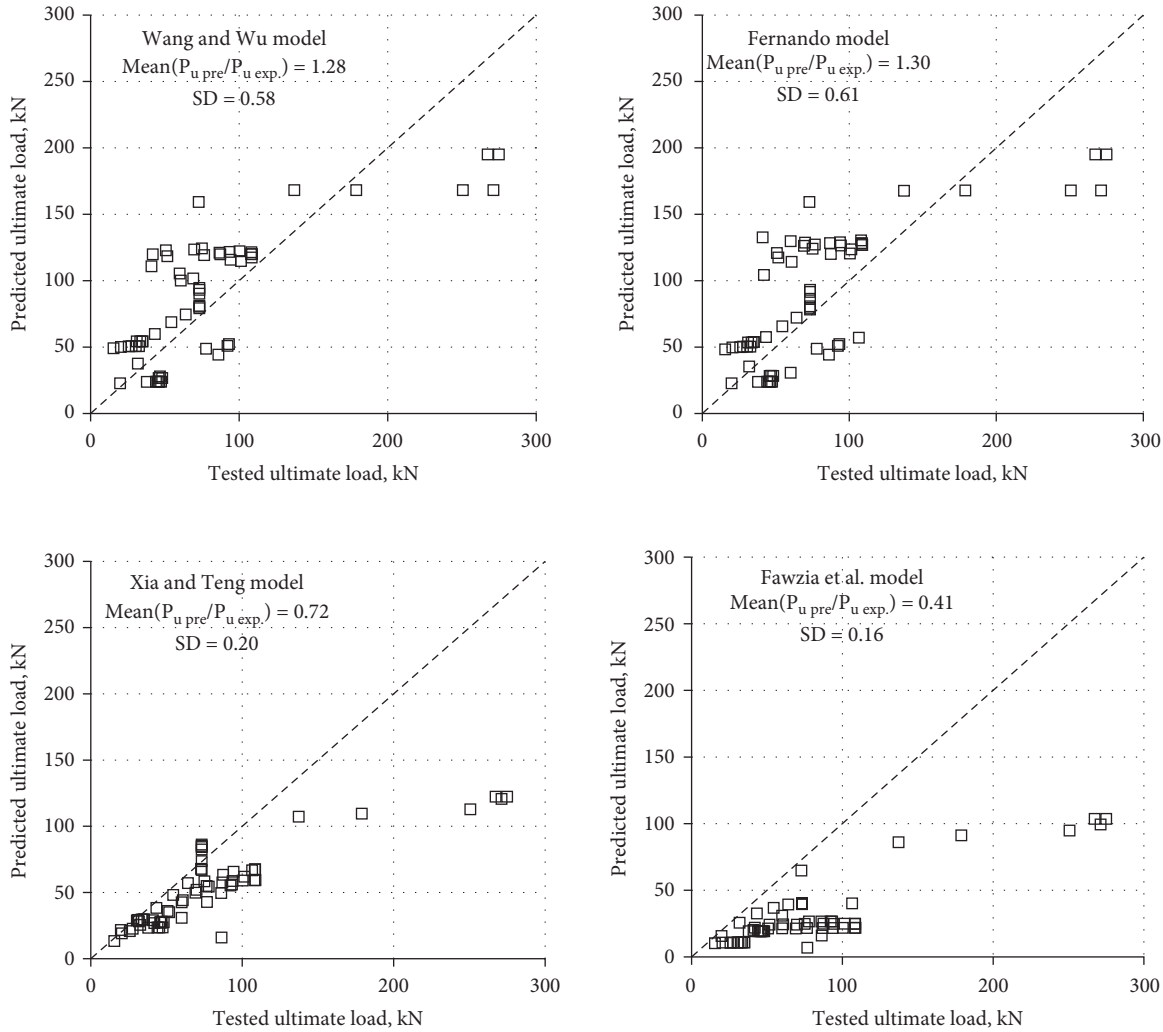

Figure 4: Comparisons of predicted vs. experimental ultimate load (Pu), evaluating existing τ–s models.

and G_t is fracture energy in the second shear direction (mode III).

5. Predictions of Existing Models

FE analysis was conducted for each of the 78 experimental samples in Table 2 to examine the accuracy of the four bond-slip models discussed in Section 2 in simulating the bond behaviour of FRP-steel joints. In implementing the FE model for evaluation purposes, the inputs required for the traction-separation law, for example, *tno*, *tso*, *tto*, and s_m, were obtained from the theoretical expressions associated with each of the examined τ–s models in Table 1. Figure 4 plots the ultimate load (Pu) comparisons from either test results or predictions of FE simulations implementing the four examined τ–s models.

FE analysis was conducted for each of the 78 experimental samples in Table 2 to examine the accuracy of the four bond-slip models discussed in Section 2 in simulating the bond behaviour of FRP-steel joints. In implementing the FE model for evaluation purposes, the inputs required for the traction-separation law, for example, t_n^o, t_s^o, t_t^o, and s_m, were obtained from the theoretical expressions associated with each of the examined τ–s models in Table 1. Figure 4 plots the ultimate load (Pu) comparisons from either test results or predictions of FE simulations implementing the four examined τ–s models.

The existing models provided a prediction of Pmax with various levels of accuracy compared with experimental results, when the mean value of predicted/tested Pu was 0.72, 0.41, 1.30, and 1.28 for the models by Xia and Teng [11], Fawzia et al. [16], Fernando [17], and Wang and Wu [18], respectively. Also, the models by Xia and Teng [11] and Fawzia et al. [16] generally underestimated Pu, while those by Fernando [17] and Wang and Wu [18] provided over predictions of Pu, but at much better accuracy. In terms of failure mode, the numerical specimens corresponding to Xia and Teng [11] and Fawzia et al.'s [16] τ–s models failed mostly by debonding, while those containing Fernando [17] and Wang and Wu's [18] expressions failed predominantly by FRP rupture. These results are contrary to the failures reported experimentally, namely, debonding, if L_f is shorter than L_{eff}, or rupture and/or cohesive otherwise. The numerical trend can be attributed to the relatively high fracture

energy of the trapezoidal models by Fernando [17] and Wang and Wu [18] (Figure 1), which allow for more stress transfer from steel to FRP to occur, delaying debonding and promoting rupture, in contrast to the other two bilinear models with low fracture energy.

Figure 5 plots the relation between Pu and L_f, as obtained from test results from Al-Mosawe et al. [19] study or FE predictions using either of the τ–s models. The existing models provided some differences from the experimental results regarding Pu and L_f relation or predict the effective bond length (L_{eff}). The Pu values corresponding to Fernando [17] and Wang and Wu [18] bond-slip models were overly predicting test results, particularly for short bond lengths. On the contrary, Xia and Teng [11] and Fawzia et al.'s [16] τ–s models yielded severe under predictions, particularly at longer bond lengths.

Figure 6 plots the experimentally and numerically extracted values of L_{eff} against FRP modulus (E_f), also for Al-Mosawe et al. [19] specimens. The experimentally reported L_{eff} was 110, 110, and 70 mm for E_f = 159.4, 203, and 457.8 Gpa, respectively. Like previous results, the τ–s models failed to predict the relation between L_{eff} and FRP moduli. Several conclusions can be drawn from the results of Figures 4–6:

(1) The diverging results from existing τ–s models necessitate the development of a new bond-slip model capable of yielding better predictions for a range of material and geometric variations.

(2) Some studies [19] found that the effective bond length is significantly affected by E_f, yet none of the existing bond-slip models considers this parameter.

(3) Existing τ–s models do not distinguish between FRP laminate (plate) and sheet. Since laminates have a larger shear deformation capacity than sheets [20], this parameter also needs further evaluation.

6. Proposed Model

In this section, a new τ–s model is proposed, aiming at overcoming the limitations of the existing models discussed earlier and providing better predictions for the interfacial behaviour of FRP-steel joints. The model was developed using a hybrid procedure that relies on experimental results, FE models, regression analysis, findings, and recommendations from literature. In utilizing the test results of Table 2, only specimens failing by debonding or cohesions were included in model development. These specimens were modelled numerically, and an inverse analysis (shown graphically in Figure 7) was implemented where for each specimen, the FE load step corresponding to Pmax from experimental results is used to extract fracture energy for the FRP-steel joint and evaluate the effects of several key variables.

Figure 8 plots the interfacial fracture energies (G_f) for several specimens in Al-Mosawe et al. [19] tests, extracted from the inverse analysis procedure, against the bond length. G_f is approximately constant across different lengths, with an average value of 17 N/mm. Furthermore, multiple studies classified G_f into two groups based on the FRP type whether

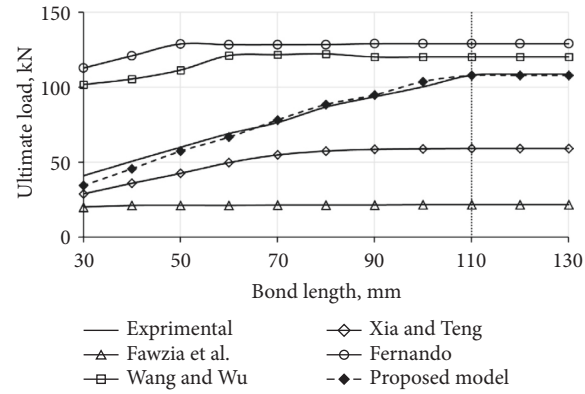

Figure 5: Ultimate load vs. bond length, comparing results from tests and FE models corresponding to existing τ–s models.

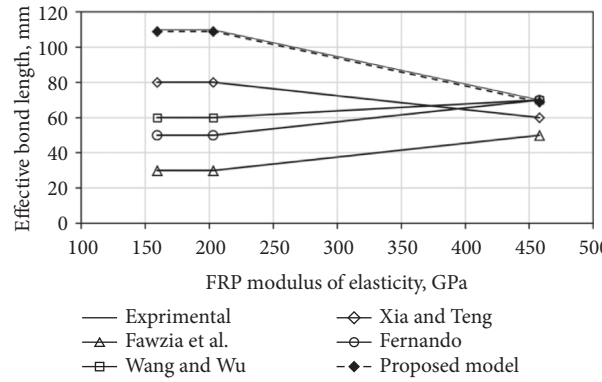

Figure 6: Effective bond length vs. FRP modulus, comparing results from tests and FE models corresponding to existing τ–s models.

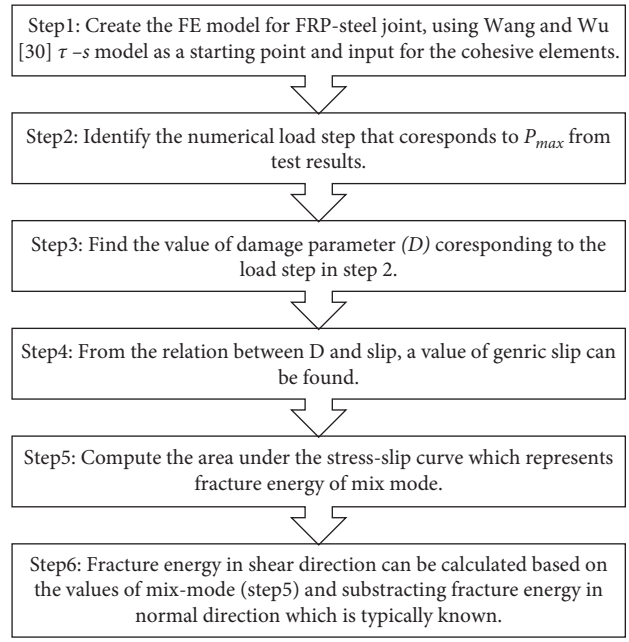

Figure 7: Inverse analysis procedure to determine the fracture energy of FRP-steel joints.

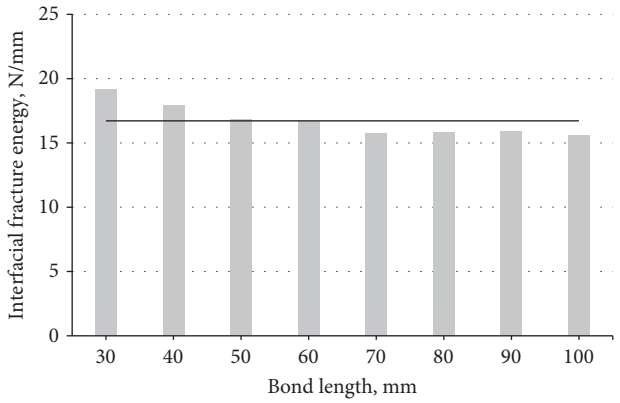

Figure 8: Interfacial fracture energy (G_f) vs. bond length (Lf), for several experimental specimens—G_f extracted from inverse analysis.

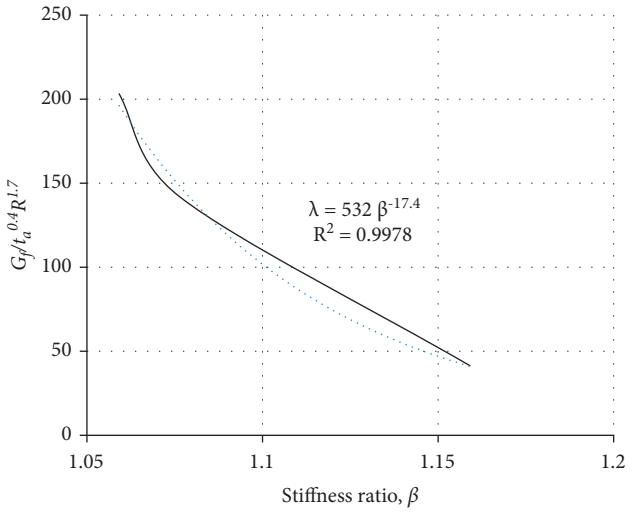

Figure 9: Relation between fracture energy (G_f) and stiffness ratio (β), and curve-fitting analysis.

it is laminate or sheet [17, 20]. For instance, Wu et al. [20] found that L_{eff} of joints with FRP laminates was longer than that with FRP sheets, likely because the former has a larger shear deformation capacity than the latter and is thicker.

(10), which is derived from regression analysis and recommendations of and will be discussed in the following sections, introduces a multiplayer (λ) to encapsulate the effects of FRP type.

$$\mathbf{G_f = \lambda t_a^{0.4} R^{1.7}}. \quad (10)$$

6.1. Effects of FRP Modulus on G_f. Numerous studies revealed that the FRP-steel bond response depends mainly on the FRP elastic modulus [13, 20]. For instance, Al-Mosawe et al. [19] found out that L_{eff} was 110 and 70 mm for normal and ultra-high modulus FRP laminates, respectively. A stiffness ratio (β) term was introduced in previous studies, which accounts for the effects of E_f on the fracture energy and general bond response of double-lap joints [18, 30], and is also adopted in the proposed τ–s model using the following equation:

$$\boldsymbol{\beta} = \frac{1}{1 - \mathbf{E_f b_f t_f / E_s b_s t_s}}. \quad (11)$$

The effect of β can be quantified by plotting the term G_f/t_a 0.4*R*1.7 versus β for different FRP types as shown in Figure 9. Based on curve-fitting analysis of the results of Figure 9, (10) can be rewritten as in equation (13).

6.2. Effects of FRP Types on G_f. The testing campaign conducted by [19] on 20 double-lap specimens with FRP sheets and addition to other tests focusing on FRP laminates is utilized in this study to characterize the effects of FRP type (sheet or laminate). Using the compiled experimental G_f data and the same curve-fitting analysis employed in Section 6.2, in addition to using G_f from (10) and dividing by those extracted from FE analysis, an additional factor (α) related to the FRP type can be obtained. α is found to be 1.0 and 0.18 for FRP laminates and sheets, respectively, showing a similar trend to several test results, which reported that L_{eff} for F sheet is less than that for FRP laminate [19, 20]. The final form for G_f can be rewritten as in (12) and includes the new two factors, α and β:

$$\mathbf{G_f = 532 \alpha \beta^{-17.4} t_a^{0.4} R^{1.7}}. \quad (12)$$

6.3. Peak Shear Stress. Analysis of experimental results and trends in Table 1 show that the peak shear stress (τ_{max}) in existing bond-slip models is unanimously related to adhesive properties, while its value only varies by a small percentage from 1 to 0.8 the adhesive tensile strength (σmax). An average value of $0.9\sigma_{max}$ is suggested in this study for τ_{max}, following the recommendations of [13, 16, 17] who conducted relatively large experimental campaigns compared with those in other studies.

6.4. Interfacial Slip. As shown in Figure 3, the interfacial slip (s) is defined by three points: (1) the maximum elastic slip (s_1) at τ_{max}, where s1 applies to both the bilinear and trapezoidal models; (2) the maximum plastic slip (s_2) also at τ_{max} for the trapezoidal model; and (3) and the slip at debonding completion (s_f) or when $\tau = 0$, applicable to both models. The following subsections discuss the proposed expressions for s_1, s_2, and s_f.

6.4.1. Maximum Elastic Slip (s1). The value for s_1 cannot be introduced into the FE model directly, but indirectly using the elastic stiffness in the shear direction and maximum shear stress as discussed previously in Section 4 and shown as follows:

$$\mathbf{s_1 = \frac{\tau_{max}}{K_s}}, \quad (13)$$

where K_s represents the stiffness in the shear direction and can be calculated as (G_a/t_a), as recommended by several FE

Table 3: Calibrated bond-slip parameters for proposed model and previous ones.

Bond-slip model		G_f (N/mm)	s_2 (mm)	s_f (mm)	s_f/s_2
Xia and Teng [11] (triangular model)		4.20	—	0.36	—
Fawzia et al. [16] (triangular model)		0.46	—	0.125	—
Fernando [17] (trapezoidal model)		37.1	0.80	2.11	2.6
Wang and Wu [18] (trapezoidal model)		22.3	0.61	1.22	2.0
Proposed model	FRP-low modulus	17.6	0.36	0.90	2.5
	FRP-normal modulus	11.4	0.23	0.58	2.5
	FRP-UH modulus	3.5	0.08	0.19	2.5

* G_f = interfacial fracture energy; s_f = slip at failure; s_2 = maximum plastic slip.

studies from the literature [18–28]. The final form for $s1$ can be written as follows:

$$\mathbf{s_1} = \frac{0.9\boldsymbol{\sigma_{max}}}{(\mathbf{G_a}/\mathbf{t_a})}. \quad (14)$$

6.4.2. Maximum Plastic Slip and Slip at Failure. Significant variation for the values of s_2 and s_f can be noticed in predictions from existing τ–s models. For instance, when these values are calculated for the specimens tested by Al-Mosawe et al. [19], they are ranged between 0.61 to 0.8 mm and 0.125 to 2.11 mm for s_2 and sf, respectively. It can be concluded from Tables 1 and 3 that the ratio of s_f/s_2 was 2.0 for Wang and Wu's [18] τ–s model and is variable in Fernando's [17] model. In addition, the research by Dehghani et al. [26], which also discussed the bond-slip behaviour of steel-FRP joints, proposed a value of 3 for s_f/s_2 ratio.

Averaging s_f/s_2 values from different experimental campaigns, a value of 2.5 is proposed herewith and provided reasonable results as will be discussed in the next sections. Using the proposed equations for G_f and τ_{max} and equating G_f to the area under either the bilinear or trapezoidal τ–s models, s2 and sf can be determined from (15) and (16), while the general shape of the proposed τ–s model is trapezoidal, which applies to nonlinear adhesives, applying (15) for linear adhesives results in s_2 value approximately equal to s_1 and returns a virtually triangular shape—indicating that it can be used for both adhesive types.

$$\mathbf{s_2} = \frac{305\boldsymbol{\alpha\beta}^{-17.4}\mathbf{t_a}^{0.4}\mathbf{R}^{1.7}}{\boldsymbol{\tau_{max}}} + \frac{\mathbf{s_1}}{3.5}, \quad (15)$$

$$\mathbf{s_f} = \frac{763\boldsymbol{\alpha\beta}^{-17.4}\mathbf{t_a}^{0.4}\mathbf{R}^{1.7}}{\boldsymbol{\tau_{max}}} + \frac{\mathbf{s_1}}{1.4}. \quad (16)$$

7. Evaluation of the Proposed Model

In this section, the predictability of the proposed model ($\tau_{max} = 0.9\ \sigma_{max}$, Equations (14)–(16)) is evaluated by implementing the model into FE analysis of FRP-steel joints and comparing the numerical results with those from experiments, a process identical to that undertaken in Section 5. To provide accurate and unbiased evaluations, the majority of experimental specimens used in this section for testing the predictability of the proposed model were different from those used in previous sections for model development. The differences were in FRP width, adhesive thickness, FRP lengths, and FRP properties. The following subsections discuss various results obtained from the model and comparisons with test data, showing the model's ability to capture the behaviour of FRP-steel joints.

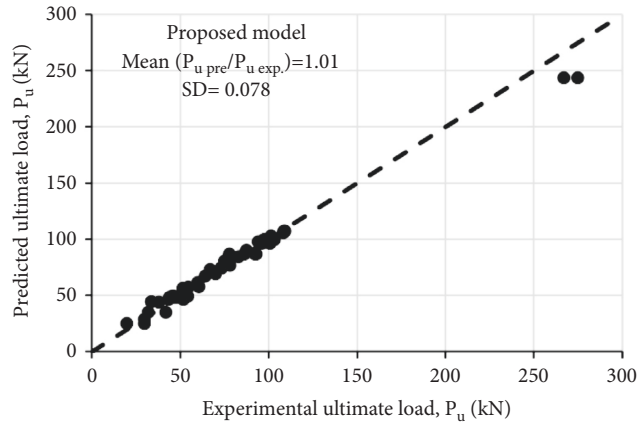

Figure 10: Comparisons of predicted vs. experimental ultimate load (Pu), evaluating proposed τ–s model.

7.1. Ultimate Load. Figure 10 plots the ultimate load (Pu) comparisons from either test results or predictions of FE simulations implementing the proposed τ–s model. It can be seen clearly that the predicted and test values of Pu are in good agreement, where the mean value of predicted (Pu pre)/experimental (Pu exp) ultimate loads is 1.01 with a standard deviation of 0.078. Compared with the Wang and Wu's [18] model, which was the best performing among the four existing models with a (Pu pre)/(Pu exp) of 1.28 and a standard deviation of 0.58 (Figure 4), the proposed model yielded much better predictions, reflecting a higher level of accuracy.

Figure 5 plots the relation between Pu and FRP-bond length (L_f) and shows that the proposed model can capture the variation of Pu with Lf, with a good level of accuracy. The model resulted in an effective bond length (L_{eff}) of 110 mm, which is identical to that reported in experiments. Figure 6 shows the relation between L_{eff} and FRP modulus (E_f), where L_{eff} is determined from test results or FE simulations corresponding to existing models and the proposed one. It can be seen from the figure that the proposed model is able of

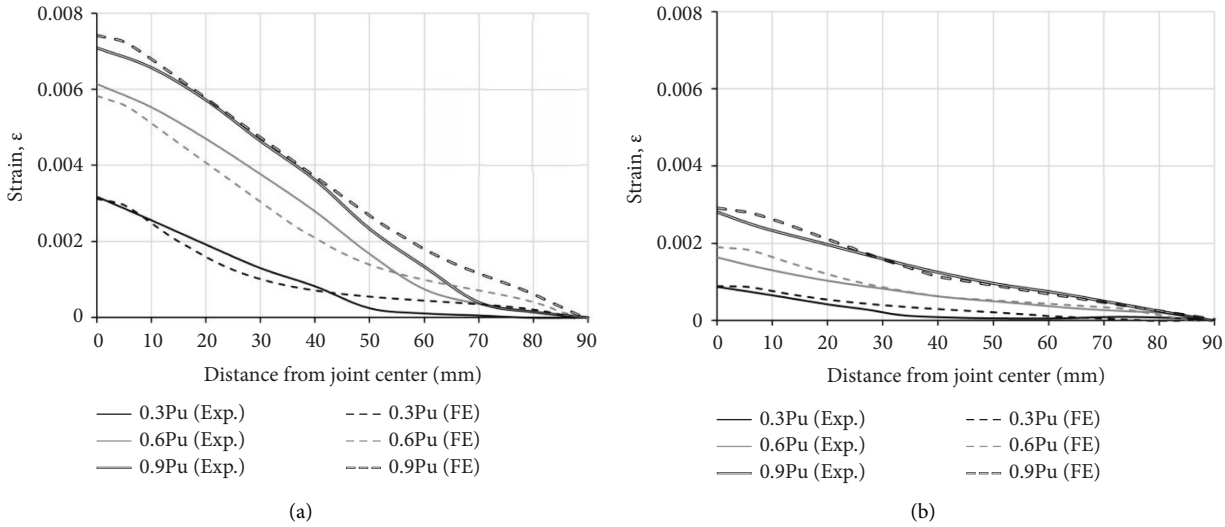

Figure 11: CFRP strains along the bond length (from the centre of joint to free end) for specimens. (a) NS-90 and (b) UHS-90.

predicting the variation of L_{eff} concerning various FRP modules (low, normal, high, ultra-high).

7.2. CFRP Strain Distribution. The bond-slip model affects the forces transferred from steel to FRP and ultimately the strains developed in the composite material. It is therefore necessary to also test the model predictions in terms of FRP strains. Figure 11 plots two representative double-lap specimens and the strains along the bond length of CFRP laminate, comparing results from the test and those from FE simulations using the proposed τ–s model. Figure 11 shows the model's ability to simulate the FRP strains at various loading levels and in different locations along with Lf, for two different FRP moduli, low in specimen NS-90 and ultra-high in specimen UHS-90.

7.3. Load-Slip Curve. The load-joint displacement (P-Δ) response provides other means of validating the predictions of the proposed bond-slip model. Figure 12 presents the P-Δ comparisons from testing and the FE model corresponding to the proposed τ–s model, for a representative specimen CF3-BL100 from Table 2. The FE-based P-Δ agreed well with that from the experiment in terms of stiffness and ultimate load, with a slightly larger, 0.57 vs. 052 mm, Δ at ultimate.

7.4. Mode of Failure. A robust bond-slip model must be able to yield similar failure modes to those observed experimentally. Figure 13 shows the FE failure progression in three representative specimens from Table 2, NS-50, NS-70, and UHS-80, from experiments and FE model corresponding to the proposed τ–s model. Figure 13(a) plots the experimental and numerical damage parameters in relation to joint displacement and shows the model's ability to trace the debonding failure along the loading path. In this figure, three points along the numerical damage parameter-displacement curve are indicated, point 1 (at no debonding), point 2 (moderate debonding), and point 3 (complete debonding).

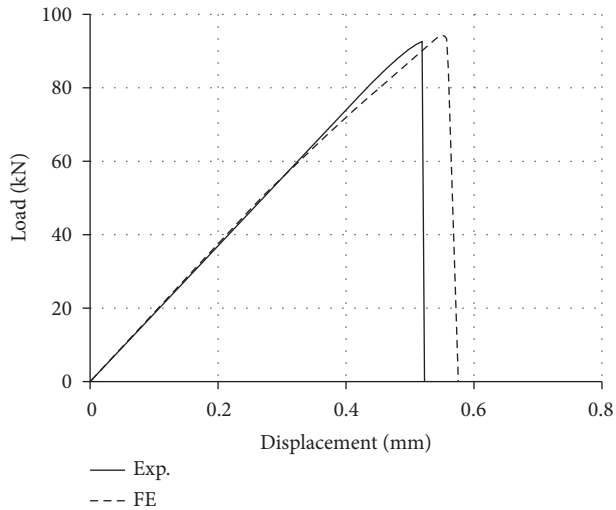

Figure 12: Comparison between experimental and FE load vs. displacement curves for specimen CF3-BL100.

The FE model corresponding to either of these three points is given in Figure 13(b), showing the physical debonding in the adhesive layer. Overall, the proposed model demonstrated a good correlation with test results, a reasonable variation with different key parameters, and superior performance compared with existing models. However, further research must be conducted to validate the model's predictions with a larger and more diverse experimental database and to carefully study the effects of two parameters found in this study to impact the τ–s model, namely, FRP type (sheet vs. laminate) and FRP modulus.

8. Beam Case Studies

In previous sections, the proposed τ–s model is evaluated against experimental results of small-scale steel-FRP joints. In this section, the model is validated against large-scale FRP-bonded beam tests, which are more realistic and

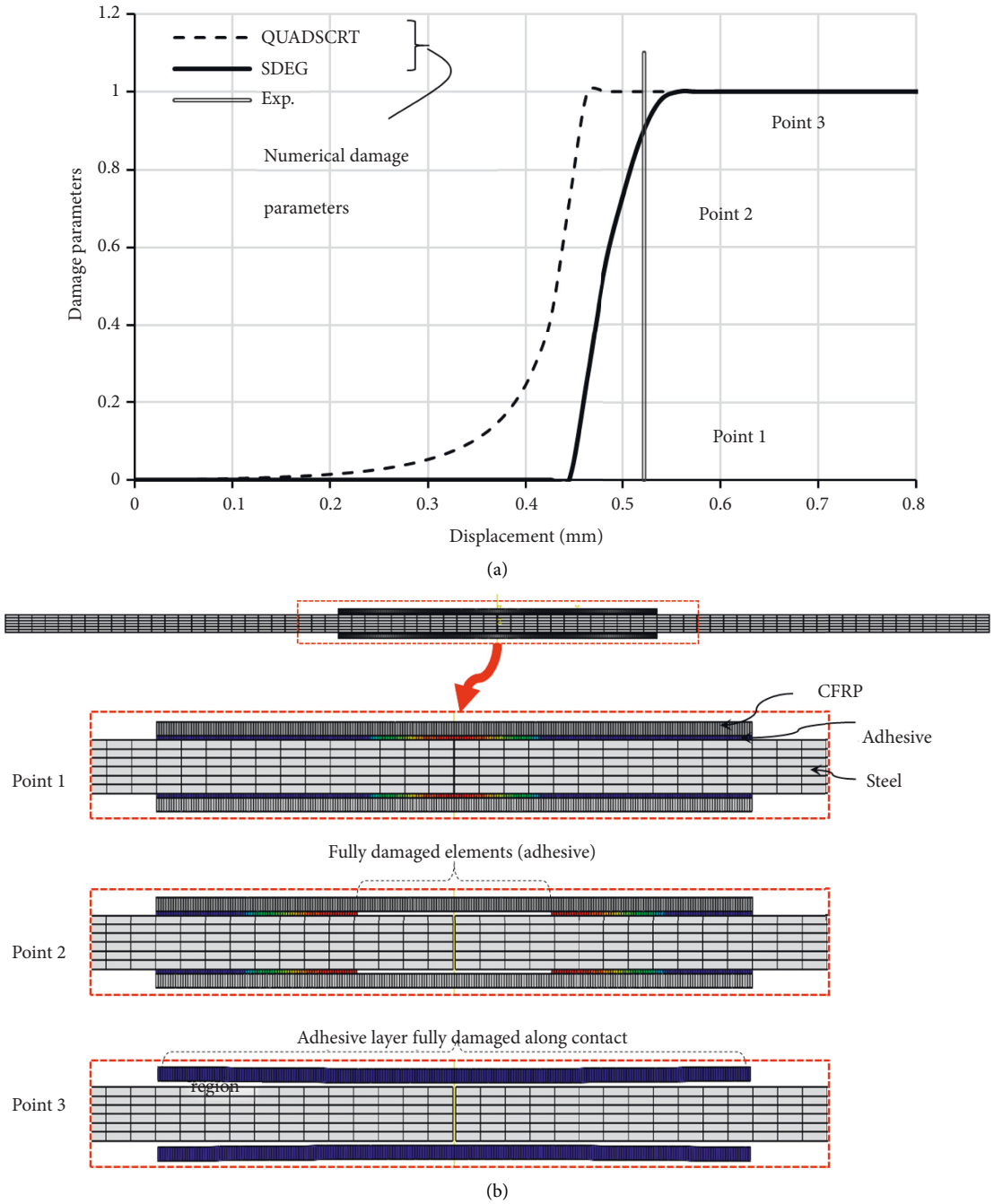

Figure 13: (a) Damage parameters vs. displacement; (b) physical damage in CFRP-steel joint under different displacement values, for specimen CF3-BL100. QUADSCRT = quadratic stress damage initiation criterion; SDEG = damage variable.

representative of field applications than single- and double-lap specimens. Two sets of beam tests are used in the validation procedure and are detailed in the following subsections. The same modelling methodology (element types, constitutive relations, loading type, etc.) that was used for the double-lap joints and discussed in previous sections is implemented herewith for the beam models.

8.1. Deng and Lee's [27] Tests. In this experimental work, three steel beams with a length of 1.2 m and a 127 × 76 UB13 section were strengthened with 3 mm thick CFRP plates and tested in flexure to failure, under three points. The primary variable in the testing campaign was the CFRP length, ranging from 300 to 500 mm, as shown in Table 3. A normal modulus, $E_f = 212$ GPa, CFRP plate was used in the tests. The adhesive material used to bond the CFRP plate to the beam soffit was Sikadur 31 (linear type), whose properties and inputs are given in Table 4.

Figure 14(a) plots the load (P) versus mid-span deflection (Δ) curves for the three tested beams and three corresponding FE models using the proposed τ–s model.

Table 4: Properties and key results of FRP-bonded steel beams, comparing experiments and FE models with the proposed τ–s model.

Specimen ID[1]	$L^{(2)}$ (mm)	P_u [2] (kN)			Δ_u [2] (mm)			Failure mode	
		Exp.	FE	%	Exp.	FE	%	Exp.	FE
S3031	300	120.0	121.2	1.0	5.12	4.68	9.4	DB 3	DB
S3041	400	135.0	134.8	0.1	7.00	7.71	9.2	DB	DB
S3051	500	149.1	141.9	5.1	12.43	11.51	8.0	DB	DB
B501	500	93.7	97.1	3.5	--	8.67	--	DB	DB
B651	650	105.9	106.6	0.7	10.06	9.44	6.6	DB	DB
B1201	1200	143.0	148.0	3.4	19.39	19.52	0.7	R 3	R

[1]Beams S303, S304, and S305 were from Deng and Lee's study [27], and beams B50, B65, and B120 were from Lenwari et al.'s study [28]. [2]L = length of CFRP plate; Pu = ultimate load; Δ = mid-span deflection at Pu. [3] DB = debonding; R = rupture of CFRP laminate.

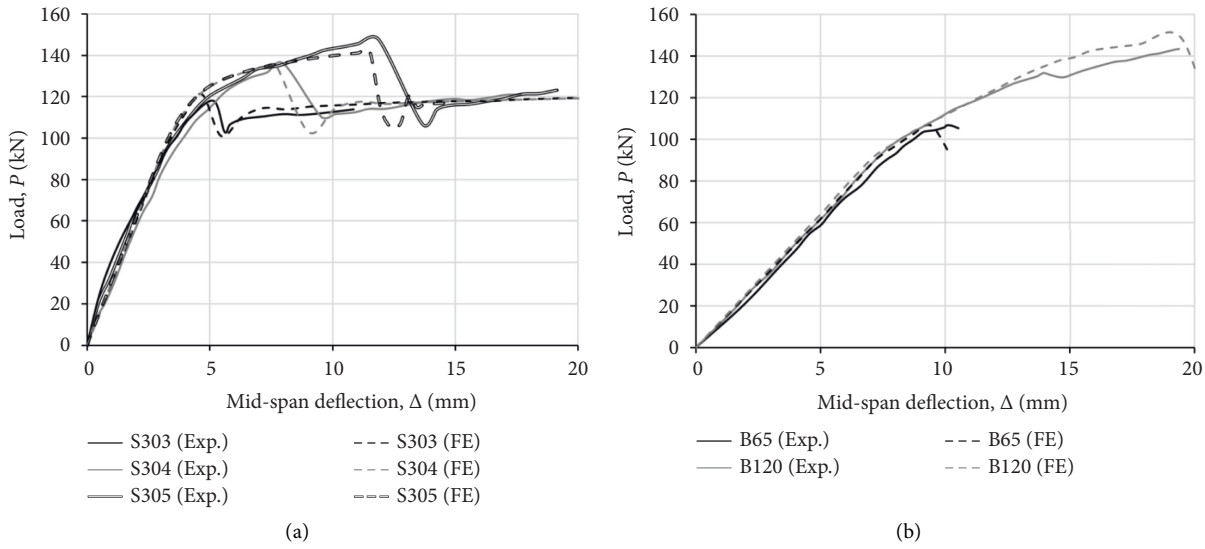

Figure 14: Load vs. mid-span deflection curves from FE models and experimental tests. (a) Deng et al. [27] and (b) Lenwari et al. [28].

The general P-Δ response from the FE models is in very good correlation with test results, and the model was able to simulate the pre- and post-yielding stiffness for each beam. The ultimate load (Pu) ratio, numerical/experimental (Pu FE/Pu Exp), varied from 5.12 to 12.43%, with an average value of 8.18% for all three beams. Similarly, the numerical/experimental ratio for the deflection at ultimate was less than 10% for all beams. The failure mode observed in tests was debonding of the CFRP laminate and was accurately simulated in the FE models, reflecting excellent correlations from the proposed τ–s model.

8.2. Lenwari et al.'s [28] Study. This study tested three steel beams, with a span of 1.8 m and a W100 × 17.2 section, strengthened in flexure by three different CFRP lengths as listed in Table 3. Steel plates, having 200 mm width and 12.2 mm thickness, were welded to the top flange of the steel beams to prevent compressive yielding. A high modulus, E_f = 300 GPa, CFRP plate with an ultimate strength of 1400 MPa was used in the study. The bonding agent between CFRP and steel was Sikadur 30 (linear type), whose properties and inputs are given in Table 4.

Figure 14(b) plots P-Δ curves for the three tested beams and three corresponding FE models using the proposed τ–s model. Like the previous tests in [27], the FE models simulated accurately the general P-Δ response and stiffness for beams B50, B65, and B120 from Lenwari et al.'s [28] study. The maximum (Pu FE/Pu Exp) ratio was less than 3.5%, indicating a close correlation for the ultimate load. The FRP rupture and debonding failures reported in [28] were both captured by the FE models. The combined results from the 6 beam specimens tested by [27, 28] confirm the capability of the proposed τ–s model to accurately represent the FRP-steel interface, leading to excellent predictions for the flexural behaviour of FRP-bond steel.

9. Conclusions

Strengthening of steel structures with fibre-reinforced polymer (FRP) composites has become a desirable option due to FRP's excellent attributes of high strength, non-corrosive nature, and ease of application. The bond between an FRP and steel, which is analytically characterized by a bond-slip (τ-s) model, plays a significant role in ensuring the effectiveness of the strengthening system. The few existing τ-s relations for FRP-steel joints are derived from diverse test setups and material properties and have different shapes and expressions, thus are expected to yield inconsistent or inaccurate results. In this study, predictions of four widely

used τ-s models are evaluated using a large experimental database of 78 double-lap experiments and finite element (FE) simulations. The following conclusions are drawn based on the results of this work:

(i) None of the existing models was able to provide a good prediction for the ultimate load (P_u) and effective bond length (L_{eff}) of FRP-steel joints. The ratio between predicted and tested Pu ranged from 0.41 to 1.3 with large standard deviations.

(ii) A new τ-s model is proposed and considers the effects of several parameters not included in existing models, namely, FRP modulus (E_f), ranging from normal to ultra-high modulus, and type of FRP reinforcement (sheet versus plate). The model takes a trapezoidal shape and applies to both linear and nonlinear adhesives.

(iii) Predictions of the proposed model were validated by comparing with results of double-lap joint tests, yielding excellent predictions for Pu, FRP strains, and failure modes. Unlike other τ-s expressions, the proposed model was able to capture the relation between Pu and bond length and that between L_{eff} and E_f.

(iv) Full-scale bending tests were also deployed to confirm the accuracy of the proposed τ-s model for actual FRP-strengthened members. The model resulted from inaccurate predictions of ultimate load, load-deflection curves, and failure modes for 6 simulated beams with different strengthening lengths, E_f, and adhesive types.

Data Availability

All data are included within the article.

Disclosure

The research was performed as part of the employment of the authors. These include (i) University of Babylon, Hilla, Iraq; (ii) Queen's University, Kingston, Canada; (iii) Al-Mustaqbal University College, 51001, Babylon, Iraq; and (iv) Lulea University of Technology, Lulea 97187, Sweden.

Conflicts of Interest

The authors declare no conflicts of interest.

References

[1] Federal Highway Administration, "National Bridge Inventory," 2014, https://www.fhwa.dot.gov/bridge/nbi.cfm.

[2] A. Peiris and I. Harik, "FRP-Steel bond study of IM and UHM CFRP strips," *Construction and Building Materials*, vol. 185, pp. 628–637, 2018.

[3] A. Fam, C. MacDougall, and A. Shaat, "Upgrading steel-concrete composite girders and repair of damaged steel beams using bonded CFRP laminates," *Thin-Walled Structures*, vol. 47, no. 10, pp. 1122–1135, 2009.

[4] A. Peiris and I. Harik, "Steel bridge girder strengthening using postinstalled shear connectors and UHM CFRP laminates," *Journal of Performance of Constructed Facilities*, ASCE, vol. 29, , 2014.

[5] M. Tavakkolizadeh and H. Saadatmanesh, "Strengthening of steel–concrete composite girders using carbon fiber reinforced polymers sheets," *Journal of Structural Engineering*, vol. 129, no. 1, pp. 30–40, 2003.

[6] A. H. Al-Saidy, F. W. Klaiber, and T. J. Wipf, "Strengthening of steel–concrete composite girders using carbon fiber reinforced polymer plates," *Construction and Building Materials*, vol. 21, no. 2, pp. 295–302, 2007.

[7] M. Dawood, S. Rizkalla, and E. Sumner, "Fatigue and overloading behavior of steel-concrete composite flexural members strengthened with high modulus CFRP materials," *Journal of Composites for Construction*, vol. 11, no. 6, pp. 659–669, 2007.

[8] M. J. Altaee, L. S. Cunningham, and M. Gillie, "Experimental investigation of CFRP strengthened steel beams with web openings," *Journal of Constructional Steel Research*, vol. 138, pp. 750–760, 2017.

[9] N. A. Peiris, *Steel Beams Strengthened with Ultra-high Modulus CFRP Laminates*, University of Kentucky, Lexington, Kentucky, 2011.

[10] D. Schnerch and S. Rizkalla, "Flexural strengthening of steel bridges with high modulus CFRP strips," *Journal of Bridge Engineering*, vol. 13, no. 2, pp. 192–201, 2008.

[11] S. H. Xia and J. G. Teng, "Behaviour of FRP-to-steel bonded joints," in *Proceedings of the International Symposium BBFS*, pp. 419–426, Hong Kong, China, December 2005.

[12] D. Schnerch, M. Dawood, S. Rizkalla, E. Sumner, and K. Stanford, "Bond behavior of CFRP strengthened steel structures," *Advances in Structural Engineering*, vol. 9, no. 6, pp. 805–817, 2006.

[13] S. Fawzia, R. Al-Mahaidi, and X. L. Zhao, "Experimental and finite element analysis of A double strap joint between steel plates and normal modulus CFRP," *Composite Structures*, vol. 75, no. 1-4, pp. 156–162, 2006.

[14] M. Bocciarelli, P. Colombi, G. Fava, and C. Poggi, "Prediction of debonding strength of tensile steel/CFRP joints using fracture mechanics and stress based criteria," *Engineering Fracture Mechanics*, vol. 76, no. 2, pp. 299–313, 2009.

[15] R. Haghani, "Analysis of adhesive joints used to bond FRP laminates to steel members-A numerical and experimental study," *Construction and Building Materials*, vol. 24, no. 11, pp. 2243–2251, 2010.

[16] S. Fawzia, X. L. Zhao, and R. Al-Mahaidi, "Bond–slip models for double lap joints strengthened by CFRP," *Composite Structures*, vol. 92, no. 9, pp. 2137–2145, 2010.

[17] N. D. Fernando, *Bond behaviour and debonding failures in CFRP strengthened steel members*, Ph.D. thesis, Hong Kong Polytechnic University, Hong Kong, China, 2010.

[18] H. T. Wang and G. Wu, "Bond-slip models for CFRP plates externally bonded to steel substrates," *Composite Structures*, vol. 184, pp. 1204–1214, 2018.

[19] A. Al-Mosawe, R. Al-Mahaidi, and X. L. Zhao, "Effect of CFRP properties on the bond characteristics between steel and CFRP laminate under quasi-static loading," *Construction and Building Materials*, vol. 98, pp. 489–501, 2015.

[20] C. Wu, X. L. Zhao, W. Hui Duan, and R. Al-Mahaidi, "Bond characteristics between ultra high modulus CFRP laminates and steel," *Thin-Walled Structures*, vol. 51, pp. 147–157, 2012.

[21] H. Al-Zubaidy, R. Al-Mahaidi, and X. L. Zhao, "Experimental investigation of bond characteristics between CFRP fabrics

and steel plate joints under impact tensile loads," *Composite Structures*, vol. 94, no. 2, pp. 510–518, 2012 Jan 1.

[22] T. C. Nguyen, Y. Bai, X. L. Zhao, and R. Al-Mahaidi, "Mechanical characterization of steel/CFRP double strap joints at elevated temperatures," *Composite Structures*, vol. 93, no. 6, pp. 1604–1612, 2011.

[23] J. G. Teng, D. Fernando, and T. Yu, "Finite element modelling of debonding failures in steel beams flexurally strengthened with CFRP laminates," *Engineering Structures*, vol. 86, pp. 213–224, 2015.

[24] SIMULIA, *Analysis User's Manual*, SIMULIA, Dassault Systems, Providence, RI, USA, 2016.

[25] Z. Hashin, "Failure criteria for unidirectional fiber composites," *Journal of Applied Mechanics*, vol. 47, no. 2, pp. 329–334, 1980.

[26] E. Dehghani, F. Daneshjoo, A. A. Aghakouchak, and N. Khaji, "A new bond-slip model for adhesive in CFRP–steel composite systems," *Engineering Structures*, vol. 34, pp. 447–454, 2012.

[27] J. Deng and M. M. Lee, "Behaviour under static loading of metallic beams reinforced with a bonded CFRP plate," *Composite Structures*, vol. 78, no. 2, pp. 232–242, 2007.

[28] A. Lenwari, T. Thepchatri, and P. Albrecht, "Flexural response of steel beams strengthened with partial-length CFRP plates," *Journal of Compos*, vol. 9, 2005.